doi:10.1038/nature12338

Imaging Solitons

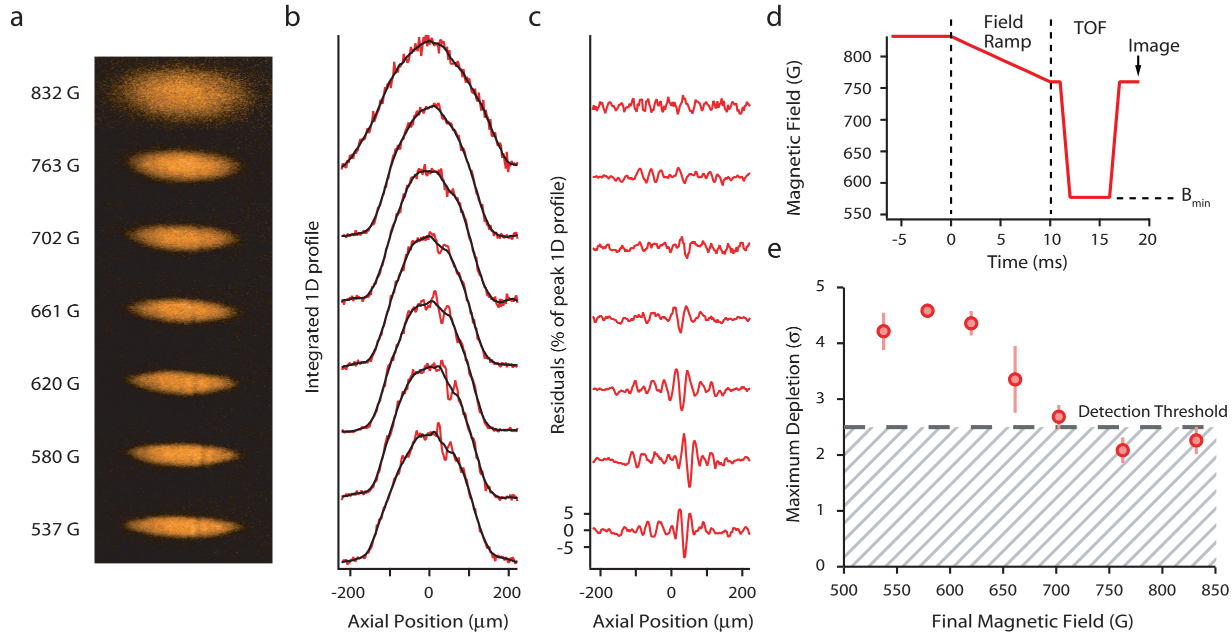

Figure S 1: **Imaging solitons. a** Optical density, **b** integrated 1D profiles and **c** corresponding residuals of a fermionic superfluid, prepared at $832\,\mathrm{G}$, after expansion and rapid ramp to various final magnetic fields B_{min}. Without any ramp, the superfluid at $832\,\mathrm{G}$, observed after 9 ms time of flight, does not show a clear signature of the soliton. A 10 ms ramp to the BEC-side before expansion at $760\,\mathrm{G}$ reduces interactions but still only reveals a very faint trace of the soliton. For $B_{\mathrm{min}} < 700\,\mathrm{G}$ the soliton is revealed. **d** Sequence of the magnetic field ramp, indicating time of flight (TOF), final ramp field B_{min} and the imaging pulse at $760\,\mathrm{G}$. **e** The maximum depletion detected in the optical density, in units of the standard deviation σ found outside the soliton. The detection threshold of 2.5 σ is indicated.

Solitons gradually fill in as the interaction strength is tuned from the BEC-regime to the BCS-regime of the crossover. Indeed, in the BCS regime only a minute fraction Δ_0/E_F of the gas is Cooper paired, and only this fraction is missing at the soliton's center, where the pair wavefunction $\Delta(z)$ is maximally depleted. The contrast in the particle density thus vanishes. Indeed, absorption images of atom clouds at the Feshbach resonance, in-situ or after expansion (Fig. S 1 a), do not show any observable ($\gtrsim 3\%$) contrast. Given our signal to noise (1 σ fluctuations corresponding to a $\sim 3\%$ density ripple) and finite resolution of 3 μm, and assuming a soliton width as found from the BdG equation [1], this gives a lower bound on the soliton filling of 91%. The BdG equations predict a filling of only 20%.

While the soliton is not visible in situ, the modulus of the pair wavefunction itself can be imaged by a rapid ramp technique similar to what was used for the observation of vortex lattices in the BEC-BCS crossover [2,3]. A magnetic field ramp to the weakly interacting BEC-regime turns large fermion pairs into molecules. An absorption image of molecules thus approximately reflects the magnitude of the fermion pair wavefunction before the ramp. In addition, the ramp reduces the interaction strength and thus increases the coherence (healing) length of the superfluid, which increases the soliton contrast and increases their width.

The rapid ramp is illustrated in Fig. S 1. Starting for example with a superfluid at the Feshbach resonance, the magnetic field is first quickly ramped over 10 ms to 760 G, on the BEC-side of the Feshbach resonance where interactions are weaker and fermion pairs are more tightly bound. Next, the cloud is released from the trap. After 1 ms, the magnetic field is rapidly ramped over 1 ms to ~ 580 G, where interactions are essentially absent and fermion pairs have fully turned into tightly bound molecules. The molecular cloud further expands for 4 ms at $580\,$G, after which the magnetic field is re-ramped over 1 ms to $760\,$G. After an additional 2 ms of expansion at 760 G, the molecules are imaged via absorption imaging.

Solitons can be identified easily in the absorption images by eye. However, to automize soliton detection we implemented the following method. For each absorption image, we first generate a residual profile by subtracting a smoothened version of the optical density profile from the actual optical density profile. We determine the standard deviation of fluctuations σ and identify a depletion in the residual profile as a soliton if its depth is greater than 2.5 σ.

We have found the rapid ramp technique necessary to reveal solitons in the strongly interacting regime, which is another indication of their strong filling, next to their slow period and enhanced relative effective mass. To show the importance of the rapid ramp, we have varied the final field of the rapid ramp B_{min} between 500 and 832 G. The depth of the maximum depletion, normalized by σ, is shown in Fig S 1. For ramp fields $B_{\mathrm{min}} < 650\,$G solitons are clearly revealed.

Speed of sound measurement

The phase imprinting not only changes the phase of the superfluid, but also perturbs the density, creating a sound wave. Fig. S 2 shows the evolution of the cloud profile during the first 100 ms after a phase imprinting pulse at the Feshbach resonance. A sound wave is seen to propagate away from the potential barrier. It disappears at the edge of the atom cloud, after about 40 ms. Adjusting for the expansion during time of flight, the speed of sound is found to be 8.8 mm/s, agreeing with the expectation for the zero-temperature speed of sound $c = \sqrt{\xi/3}\,v_F$ with $\xi = 0.37$, to within 2%. Note that the soliton sequences shown in the main text start 400 ms after the phase imprint, long after the initial sound wave has disappeared.

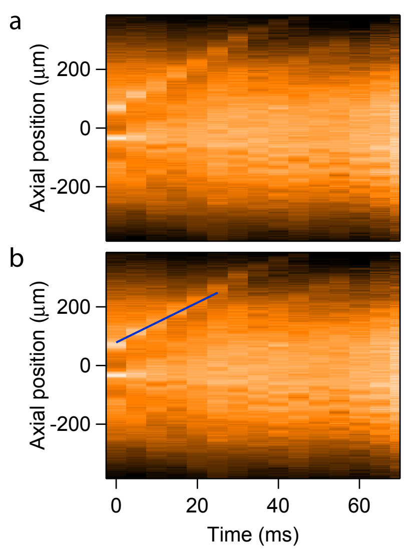

Figure S 2: **Speed of sound measurement.** **a** Integrated 1D density profiles after rapid ramp and time of flight, for the first 100 ms after applying the phase imprinting pulse at the Feshbach resonance, at 832 G. A sound wave is clearly observed. **b** same as a), with a line marking the sound wave.

Snake Instability

Planar solitons in three dimensions are not only thermodynamically unstable towards accelerating, but also dynamically unstable towards shape excitations - the so-called "snake" instability [4–8]. This excitation of the soliton plane along the radial direction grows exponentially until the soliton decays into vortices. This is suppressed in elongated trap geometries. In weakly interacting BECs, solitons are expected to become dynamically unstable when the chemical potential μ of the condensate becomes larger than $\approx 2.4\hbar\omega_\perp$, where $\omega_\perp$ is the radial trapping frequency [4]. The solitons in our strongly interacting fermionic superfluid appear to be much more robust, as they are long-lived even when the chemical potential $\mu \approx 35\hbar\omega_\perp$. Still, we were able to observe the snake instability by reducing the trap aspect ratio to about 3. Examples are shown in Fig. S 3 where the depletion revealed by the rapid ramp no longer follows a straight line but rather a wavy trajectory, characteristic of the snake instability [6–8].

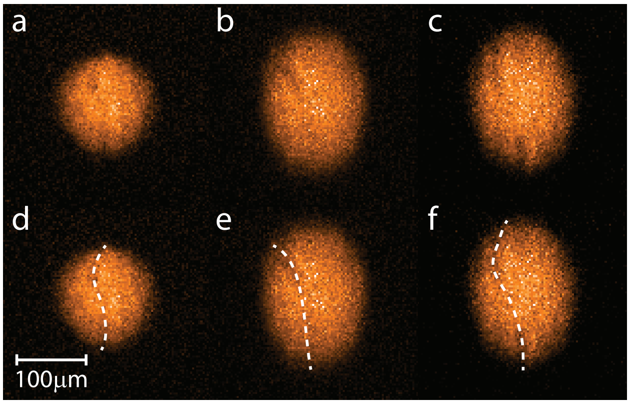

Figure S 3: **Observation of the snake instability in a fermionic superfluid. a-c** Absorption images exhibiting "snaking" solitons in expanding fermionic superfluids. **d-f** Same as a-c) but with a white dashed line as guide to the eye. The superfluids were prepared at $B = 760\,\mathrm{G}$ in a trap with aspect ratio of 2.9 (a) and 3.1 (b-c) with an axial trapping period of $T_z = 44\,\mathrm{ms}$. The images were taken $200\,\mathrm{ms}$ after the phase imprint of the soliton, using the standard rapid ramp to $B_{\mathrm{min}} = 580\,\mathrm{G}$ and a total time of flight of $9\,\mathrm{ms}$.

From Bogoliubov-de Gennes to the Andreev equation

In the BCS limit of weak attractive interactions, there exists a direct connection to solitons studied in relativistic quantum field theory [9,10] and conducting polymers [11]. Here the size of the Andreev bound state becomes much larger than the interparticle spacing, and its energy much smaller than the pairing gap. In this limit, following Andreev [12], one may separate out the fast oscillation at $k_\mu = \sqrt{\frac{2m\mu}{\hbar^2}}$ in Eq. 1 of the main text by writing $u_n(z) = u_{n0}(z)e^{\pm ik_\mu z}$, $v_n(z) = v_{n0}(z)e^{\pm ik_\mu z}$ ($\pm$ for fermions moving to the right or left), and assuming the envelope functions $u_{n0}(z)$, $v_{n0}(z)$ to be slowly varying. Then the Bogoliubov-de Gennes equation simplifies to the Andreev equation [12], a Dirac equation where the pair wavefunction $\Delta(z)$ plays the role of a spatially varying mass coupling particles and holes [9]. For vanishing transverse momentum it reads [13]:

$$\left(\mp i\hbar v_F \sigma_z \frac{\partial}{\partial z} + \Delta(z)\sigma_x\right)\begin{pmatrix} u_{n0} \\ v_{n0}\end{pmatrix} = E_n \begin{pmatrix} u_{n0} \\ v_{n0}\end{pmatrix} \tag{1}$$

Here $v_F = \frac{\hbar k_F}{m}$ is the Fermi velocity and $k_F = (3\pi^2 n)^{1/3}$ is the Fermi wavevector related to the total density n. When $\Delta(z)$ changes sign, this equation allows for one normalisable zero-energy mode for each of the Fermi points at $\pm k_\mu$, localised at the zero crossing of the gap [9]. This limiting case of an Andreev bound state, a superposition of half a particle and half a hole, famously carries half-integer particle number [9] and gives rise to the conductivity of polymers [11]. A self-consistent solution for the pairing gap is [11] $\Delta(z) = \Delta_0 \tanh(z/\xi_{\mathrm{BCS}})$, where Δ_0 is the bulk pairing gap and $\xi_{\mathrm{BCS}} = \frac{\hbar v_F}{\Delta_0}$ is the BCS coherence length. In a BCS superfluid, the Andreev bound state energy is never strictly zero owing to the non-vanishing kinetic energy cost $\hbar^2/m\xi_{\mathrm{BCS}}^2 \sim \Delta_0^2/E_F$ of forming the bound state [14,15], where $E_F = \frac{\hbar^2 k_F^2}{2m}$ is the Fermi energy.

In the theory of conducting polymers [11], $\Delta(z)$ describes the ion displacement and is a real quantity. This leads to topologically protected solitons. In the present case, $\Delta(z)$ is self-consistently related to the particle and hole amplitudes and can be complex. The state with soliton can thus be continuously deformed into the uniform state without soliton; the soliton is thus not topologically protected.

1. Antezza, M., Dalfovo, F., Pitaevskii, L. P. & Stringari, S. Dark solitons in a superfluid Fermi gas. *Phys. Rev. A* **76**, 043610 (2007).

2. Zwierlein, M. W., Abo-Shaeer, J. R., Schirotzek, A., Schunck, C. H. & Ketterle, W. Vortices and superfluidity in a strongly interacting Fermi gas. *Nature* **435**, 1047–1051 (2005).

3. Ketterle, W. & Zwierlein, M. Making, probing and understanding ultracold Fermi gases. *Rivista del Nuovo Cimento* **31**, 247–422 (2008).

4. Muryshev, A. E., van Linden van den Heuvell, H. B. & Shlyapnikov, G. V. Stability of standing matter waves in a trap. *Phys. Rev. A* **60**, R2665–R2668 (1999).

5. Feder, D. L., Pindzola, M. S., Collins, L. A., Schneider, B. I. & Clark, C. W. Dark-soliton states of bose-einstein condensates in anisotropic traps. *Phys. Rev. A* **62**, 053606 (2000).

6. Anderson, B. P. *et al.* Watching dark solitons decay into vortex rings in a Bose-Einstein condensate. *Phys. Rev. Lett.* **86**, 2926–2929 (2001).

7. Dutton, Z., Budde, M., Slowe, C. & Hau, L. V. Observation of quantum shock waves created with ultra-compressed slow light pulses in a Bose-Einstein condensate. *Science* **293**, 663–668 (2001).

8. Frantzeskakis, D. J. Dark solitons in atomic Bose-Einstein condensates: from theory to experiments. *Journal of Physics A: Mathematical and Theoretical* **43**, 213001 (2010).

9. Jackiw, R. & Rebbi, C. Solitons with fermion number 1/2. *Phys. Rev. D* **13**, 3398–3409 (1976).

10. Goldstone, J. & Wilczek, F. Fractional quantum numbers on solitons. *Phys. Rev. Lett.* **47**, 986–989 (1981).

11. Heeger, A. J., Kivelson, S., Schrieffer, J. R. & Su, W. P. Solitons in conducting polymers. *Rev. Mod. Phys.* **60**, 781–850 (1988).

12. Andreev, A. F. The thermal conductivity of the intermediate state in superconductors. *Sov. Phys. JETP, 19, 1228 (1964)* **46**, 1823 (1964).

13. Radzihovsky, L. Fluctuations and phase transitions in Larkin-Ovchinnikov liquid-crystal states of a population-imbalanced resonant Fermi gas. *Phys. Rev. A* **84**, 023611 (2011).

14. Caroli, C., Gennes, P. d. & Matricon, J. Bound fermion states on a vortex line in a type II superconductor. *Phys. Lett.* **9**, 307 (1964).

15. Yoshida, N. & Yip, S. K. Larkin-Ovchinnikov state in resonant Fermi gas. *Phys. Rev. A* **75**, 063601 (2007).